Rivers and Melt: Exploring how physical processes are stored in the geological record

John Armitage[1]

[1]IFP Energies Nouvelles, France

HDR soutenance 20/5/2021

My background

- PhD in Geophysics - National Oceanography Centre, University of Southampton, UK
  Title ‘How Does Melting Affect Continental Rift Development ?’
  2004 - 2009
- Masters in Oceanography - National Oceanography Centre, University of Southampton, UK
  Masters Project Title ‘Dissolution of Silica from Antarctic Continental Shelf Sea Sediments’
  2003 - 2004

Research Positions

Postdoc, 2009-2011
Imperial College London

Vol 448,27 June 2007 doi:10.1038/nature06043

LETTERS

The importance of rift history for volcanic margin formation

John J. Armitage*, Jenny S. Collier* & Tim A. Minshull*

Rifting and magmatism are fundamental geological processes that shape the surface of our planet. A relationship between the two is widely acknowledged but its precise nature has eluded geoscientists for decades. Volcanic rocks dredged from the ocean floor in the North Atlantic Ocean, mantle temperature was identified as the primary factor controlling magmatic production,[1] with most authors seeking to explain observed variations in volcanic activity or rifted margins in terms of the mantle temperature at the time of rifting.[2–4] Alternative explanations, however, have been made at other rifted margins worldwide; the validity of this interpretation and the importance of other factors in controlling the volume of rift-related magmatism are thus in question. We address these issues by considering the North Atlantic Ocean, where, despite an unequivocal link between an ancient flood basalt province, centred on Iceland, and the North Atlantic Igneous Province (rifted volcanic rifts associated with continental margins) no clear link exists.[5] Here we reconcile these observations by applying a numerical model that accounts explicitly for the effects of melt extraction and migration. Our approach allows us to decify compositional and thermal anomalies in the mantle that are not detectable by deep-penetrating seismic. We show that the volume of rift-related magmatism generated, both in the northwest Indian Ocean and at the Iceland hotspot, is a function of the rate of change of the mantle temperature rather than the absolute temperature, to a similar degree, on the rift history. The inferred extensional history can either suppress or enhance melt generation, which can explain previously enigmatic observations.

Extensive uncertainty in the North Atlantic have shown that the volume of rift-related magmatism can be significantly enhanced by episodes of igneous activity, such large magmatic events are potentially highly significant to the Earth's history, and have been linked to environmental change, mass extinctions, and the formation of extensive volcanic margins, spread laterally over distances of 1,000 km with spatial and temporal relationships suggesting a direct link between the two. Such a link between rifting and magmatism is explained using a model of melt generation beneath an extensive, linear extension. The calculations[1] showed little dependence on the initial lithospheric thickness when full break-up occurred and it was concluded that the primary constraint on magmatism was mantle temperature. Subsequent studies of other rifted margins worldwide have sought the relationship between high mantle temperature and voluminous magmatism beneath divergent[2–4]. It has therefore been widely accepted that the volume of rift-related magmatism is a function of the potential or excess margin, with the volume of melt decreasing steadily along strike away from the hot-spot centre.[2]. Subsequent challenges to this model have shown that the volume of magmatism is not a function of a hot spot at the time of break-up is disputed[6], or when capitalizing under variations in magmatism can observed[7,8]. However focus on new observations from the northwest Indian Ocean, where, despite an unequivocal link between an underlying flood basalt province, centred on Iceland, and the North Atlantic Igneous Province (rifted volcanic rifts associated with continental margins) no clear link exists.[5]. Here we reconcile these observations by applying a numerical model that accounts explicitly for the effects of melt extraction and migration. Our approach allows us to decify compositional and thermal anomalies in the mantle that are not detectable by deep-penetrating seismic. We show that the volume of rift-related magmatism generated, both in the northwest Indian Ocean and at the Iceland hotspot, is a function of the rate of change of the mantle temperature rather than the absolute temperature, to a similar degree, on the rift history. The inferred extensional history can either suppress or enhance melt generation, which can explain previously enigmatic observations.

Marie Curie Research Fellowship, 2011-2013
Intitut de Physique du Globe de Paris

JOURNAL OF GEOPHYSICAL RESEARCH, VOL. 117, B12405, doi:10.1029/2012JB009017, 2012

Low seismic velocities below mid-ocean ridges: Attenuation versus melt retention

Saskia Goes,[1] John Armitage,[2] Nick Harmon,[3] Hannah Smith,[3] and Rhian Huismans[1]

Received 18 July 2012; revised 3 October 2012; accepted 11 October 2012; published 13 December 2012

[1] The first comprehensive seismic component tomography subridge mantle revealed a pronounced low velocity zone between 48 and 180 km depth below the East Pacific Rise (EPR) at 9–10°N, which is interpreted as a partially molten upwelling. [2] We ask if such high melt fractions are at odds with low melt productivity and low melt retentivity inferred from petrology and geochemistry. Here, we evaluate whether seismic attenuation can reconcile subridge seismic structure with low melt fractions. We start from a dynamic spreading model which includes melt generation and migration and is converted into seismic structure, accounting for temperature, composition, melt content, melt and melt-dependent anelasticity, and melt geometry. [3] We find that melt fractions of 0.5–1% are required to explain observed attenuation, a double low-velocity zone, a shallow—approximately triangular—low velocity zone, and a low-velocity channel between 60 and 150 km depth dominantly controlled by solid state high-temperature seismic attenuation in a damp mantle, with only a minor contribution of <0.1% melt. We test how tomographic inversions influences the imaging of our model structure. We find that the low-velocity zone is well resolved in tomographic inversions, but most tomographic models only resolve the deeper velocity minimum. Experimentally constrained anelasticity formulations produce V_p as low as observed and can explain lateral variations in near-ridge attenuation/V_p with <100 K temperature variations and/or zero to high water content. Furthermore, such Q_P formulations also explain the observed lack of a low-velocity zone in teleseismic tomography and lithosphere cooling models. Although these structures are compatible with global Q_P images, they are more attenuating than permitted by EPR data.

Citation: Goes, S., J. Armitage, N. Harmon, H. Smith, and R. Huismans (2012), Low seismic velocities below mid-ocean ridges: Attenuation versus melt retention, *J. Geophys. Res.*, *117*, B12405, doi:10.1029/2012JB009017.

1. Introduction

[1] Plate creation at mid-ocean ridges is often regarded as the simplest and best understood of plate tectonic processes, with upwelling beneath the ridge axis, melting due to decompression, in response to spreading of the plates. However, the few regional seismic images of the mantle below a ridge reveal surprising complexity. The MELT experiment across a section of the East Pacific Rise (EPR) confirmed there was deep melting, but showed a pronounced low velocity zone with complex spatial variations [*Forsyth et al.*, 1998]. However, the combined data from the MELT and GLIMPSE experiments along the southern EPR, and data from an equal Californian, revealed three-dimensional anomalies that are often not centered below the ridge axis, and are not symmetrical [*Wanamaker et al.*, 2007]. The data have proposed to reflect a dynamic ridge system, with melt focusing and migration observed at the eastern North American margin, suggesting that the tilting and episodic uplift and subsidence at continental passive margins are a natural consequence of the evolution of continental lithosphere after breakup and during mature seafloor spreading.

Citation: Armitage, J. J., C. Jacquet, L. Fournel, and P. A. Allen (2013), The instability of continental passive margins and its effect on continental topography and heat flow, *J. Geophys. Res. Solid Earth*, *118*, 1817–1836, doi:10.1002/jgrb.50097.

1. Introduction

[1] It has long been recognized that the continents have a wide range of topography and elevation, with large lateral variations in the degree of continental mandelates [*Bird*, 1963]. Continental margins and adjacent plate interiors preserve a record of large-scale movements of the surface of the Earth in their stratigraphic records. In some examples, the rate of change of topography and the rate of change of sea-level can be followed by episodes of variable subsidence and erosion at a smaller wavelength (Figure 1) [*Allen and Allen*, 2005; *Cloetingh et al.*, 2005]. Such observations underpin the plate tectonic theory [*Jaupart et al.*, 1978; *Jaupart et al.*, 2012; *Allen* [*Morley and Allen*, 1994; *Crosby et al.*, 2010; *Kadima Kalunga et al.*, 2011; *Baker et al.*, 2012]; North America [*Miller et al.*, 1982; *Haig and Sexton*, 1988; *Cuddy and Graves*, 1995; *Burgess et al.*, 1997]; and Australia [*Sandiford et al.*, 1997; *Shaw et al.*, 1999; *Sandiford*, 2003], contain a long record of this ever-changing topography.

[2] The duration of subsidence within intracratonic basins is not randomly distributed through time [*Allen and Allen*, 2005; *Cloetingh et al.*, 2005]. Instead, the stratigraphic records of basin formation that cluster around times of supercontinent breakup and dispersal. Over the last billion years, the Earth has seen two supercontinent breakup events, the first being that have been the main periods of basin formation during the Cambrian to Ordovician and during the Permian to Triassic [*Allen and Armitage*, 2012]. In particular, the North American basins (Oklahoma, Illinois, Michigan) formed in the Cambrian to Ordovician, and subsided slowly toward the oceans, sum in the epoch pattern of the latest Proterozoic-Early Ordovician "Sauk" sequence of eastern North America (Figure 1a) [*Bond*, 1969]. In a similar time, the North African region was one extensive rising, increasing in elevation and subsidence [*Bond*, 1969; *Bond*, 1978; *Burgess et al.*, 1990]. The broad regional tilting of the continent toward the oceanic domain may be a generic feature of continental lithosphere after breakup and during mature spreading [*Allen and Armitage*, 2012]. Contents basins have initiated and become the result in battery-shaped depressions we observe today. These large continental basins and continental platforms have experienced a long history of episodic subsidence. Some periods of increased subsidence have been

nature geoscience LETTERS PUBLISHED ONLINE: 27 FEBRUARY 2011 | DOI: 10.1038/NGEO1097

Transformation of tectonic and climatic signals from source to sedimentary archive

John J. Armitage*, Robert A. Duller, Alex C. Whittaker and Philip A. Allen

The Earth's sedimentary successions are a mixture of geodynamic and climate events[1]. The physical characteristics of the sediment record are controlled by three main factors: the sediment supply from the eroding source region, the transport and deposition of sediment, and the accommodation available for sediment accumulation in the downstream regions[2]. The interplay of these factors can make the interpretation of the sedimentary record difficult, particularly in climate precursors to continents. Here we assess the evolution of a tectonically active landscape undergoing climate-induced variations in precipitation, and the resulting sediment transportation variations in grain size and the volumetric sediment budget. Our simulations indicate that changes in precipitation can be recorded in the sediment budget, and the pattern of grain size and stratigraphic geometry. An increase in catchment precipitation results in the deposition of a laterally extensive sheet of coarse grained sediment. The response to a changing tectonic regime are more diverse a large increase in uplift rate results in a coarsening of the sediment and a change in grain size at proximal sites, followed by a reduction in grain size at distal locations. We conclude that the stratigraphic record is a complex mixture of tectonic and climatic signals, and that interpretations of stratigraphy in terms of climatic change, should be made with caution.

The sedimentary response to motion of an upland source region is controlled by the interplay between tectonic, climatic and spatial scales[1]. Over geological timescales, the architecture and geometry of fluvial successions are dependent on the accommodation available for sediment deposition, and the sediment preliminarily stored for those key parameters is non-trivial[2]. A large number of theoretical and field studies[3–7] have demonstrated that tectonic, climatic, erosion and deposition are dominantly linked by a sediment routing system, which relates source signals to sedimentary records. Numerical models of sediment routing systems[8–11] and field investigations have provided valuable but qualitative interpretations of the stratigraphic impact of tectonic and climatic forcing on sedimentary systems.

Two strands of forward modelling have been used to explore the landscape response to climatic and tectonic change. The first strand of research has used cellular models of landscape evolution to develop a quasi-realistic modelling landscape (for example, [12]). These studies embed field-derived lithology, fluvial and sediment transport laws, but are typically focused on relatively short time geomorphological timescales, rather than on the erosion and deposition of sediment downstream. The second strand of research has focused on geomorphological laws on which such models are built are often poorly constrained or unknowable for ancient landscapes (for example, [13]). Although the aim of the second strand, here, is to parameterize the erosional system using a nonlinear differential model that can describe the gross characteristics of topographic evolution and sediment flux that relate to the Earth's tectonic, climatic, or anthropogenic forcing, the aim is to provide a simple, but robust, model that can be used to explore the Earth's tectonic, climatic, or anthropogenic forcing. Such a model is ideal for exploring the sensitivity of the sedimentary record to changes in tectonic and climatic forcing, and to provide a framework for the interpretation of the sedimentary record in terms of tectonic and climatic forcing.

Department of Earth Science and Engineering, Imperial College London, South Kensington Campus, London SW7 2AZ, UK, *email: j.armitage@imperial.ac.uk

NATURE GEOSCIENCE VOL 4 | APRIL 2011 | www.nature.com/naturegeoscience 239 © 2011 Macmillan Publishers Limited. All rights reserved

Research Positions

Royal Astronomical Society Fellowship 2013-2015
Royal Holloway, University of London

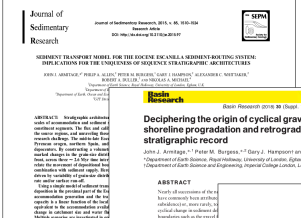

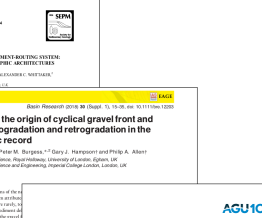

ANR Accueil de Chercheurs.es de haut Niveau 2015-2019
Institut de Physique du Globe de Paris

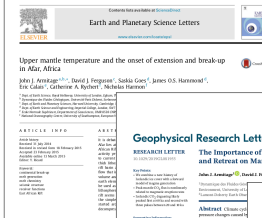

Got a job in DevOps

This badge was issued to John Armitage on 24 January 2020.
Expires on 24 January 2023

Verify

Type: Certification

Level: Intermediate

Time: Months

Cost: Paid

Additional Details

CKAD: Certified Kubernetes Application Developer

Issued by The Linux Foundation

Earners of this designation demonstrated the skills, knowledge and competencies to perform the responsibilities of a Kubernetes Application Developer. Earners are able to define application resources and use core primitives to build, monitor, and troubleshoot scalable applications and tools in Kubernetes. The skills and knowledge demonstrated by earners include Core Concepts, Configuration, Multi-Container Pods, Observability, Pod Design, Services & Networking, State Persistence.

Skills

cloud native applications | ConfigMaps | Containers | Docker | Java | Kubernetes | Node.js | Open Source Software | Orchestration | Python | rkt | Secrets | Software Developer | Volumes

Earning Criteria

- Score a passing grade on a 2-hour online, proctored performance based exam. The exam consists of a set of performance-based items (problems) to be solved in a command line, running Kubernetes.

Evidence

Certificate ID Number
CKAD-2000-002613-0100

- Develop novel methods for sediment transport for applications from risk management to exploration

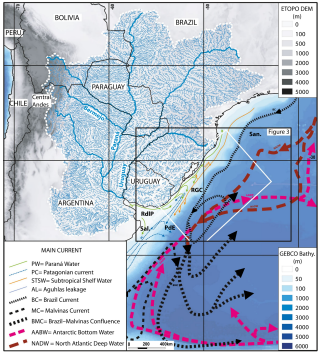

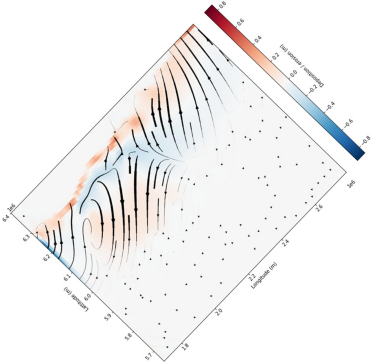

- Explore the linking between surface and sub-surface processes

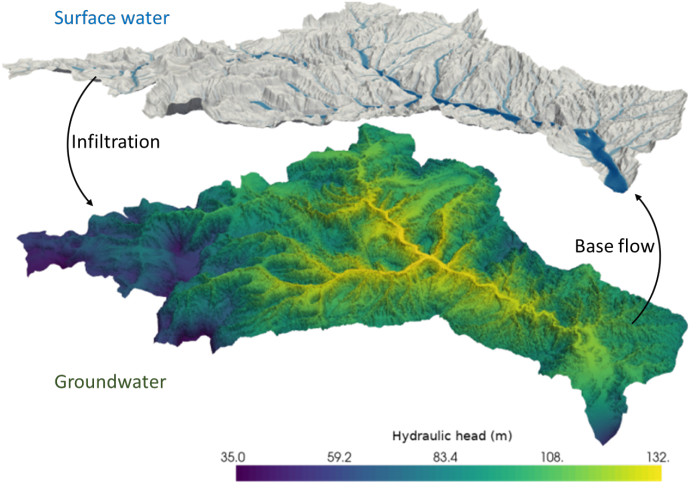

A career in numbers

- **2020 - present** Ingénieur de Recherche at IFP Energies Nouvelles
- **37** Publications
- **3** PhD students supervised:
  2012-2017: Chandra Taposeea - co-supervised with Jenny Collier, Imperial College London.
  2014-2018: Sam Brooke - co-supervised with Alex Whittaker, Imperial College London.
  2016-2019: Thijs Franken - co-supervised with Nobu Fuji & Alexandre Fournier, IPGP.
- **1** PhD student starting:
  2021-2024: Groundwater project with Niels Hovius & Christoff Andremann, GFZ
- **3** Research grants:
  EU Marie Curie Fellowship, Royal Astronomical Society Research Fellowship, ANR Acceuil de chercheurs·es de haute niveau.

Part 1: Melt

Part 1.1: Upper mantle structure below zones of volcanism

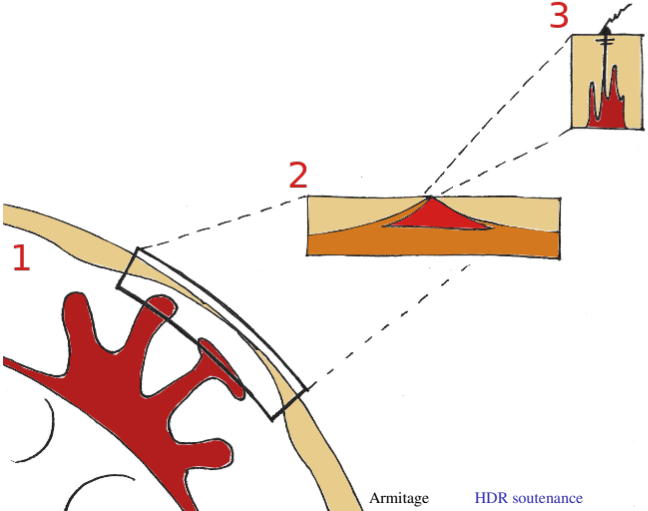

Elevated mantle temperature leads to volcanism

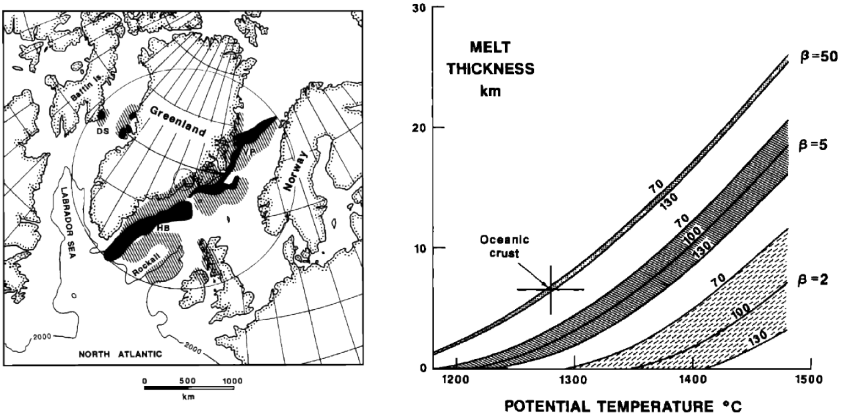

Figure: North Atlantic volcanism is because the mantle was hot (White and McKenzie, 1995).

Northern East African Rift

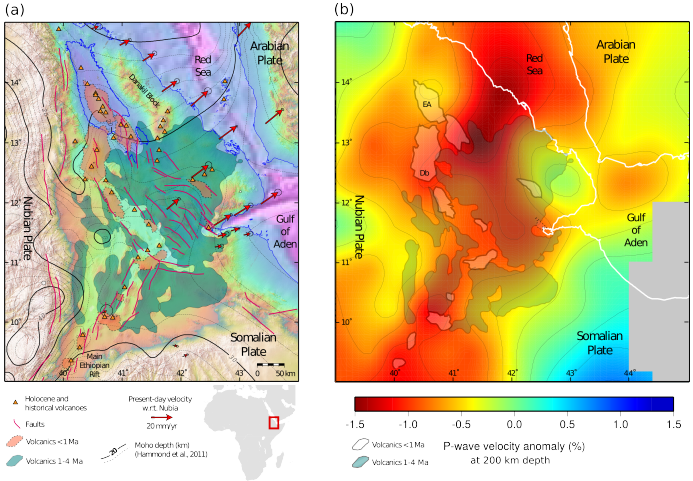

Figure: Location of basaltic intrusions and lava flows correlate with deep low seismic velocity anomalies.

Seismic structure below the Northern East African Rift

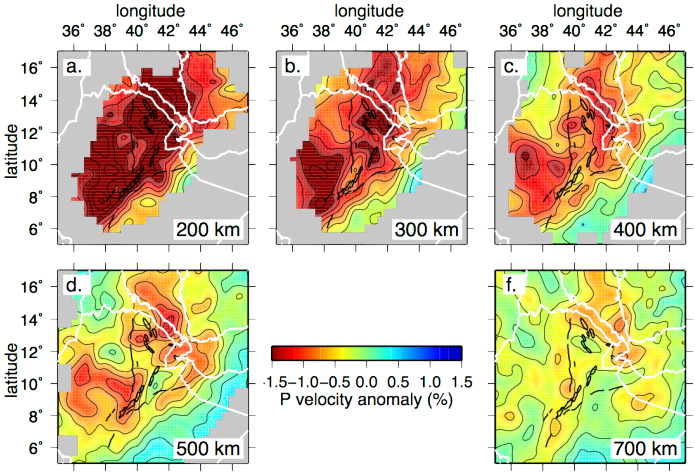

Figure: The tomographic model of Civiero et al. (2016) suggests multiple upper mantle instabilities

Seismic structure below the Northern East African Rift

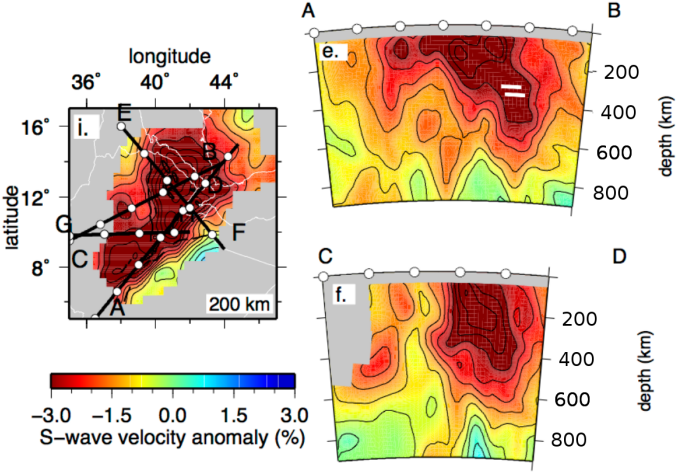

Figure: The tomographic model of Civiero et al. (2016) suggests multiple upper mantle instabilities

Secondary plumes or destabilisation?

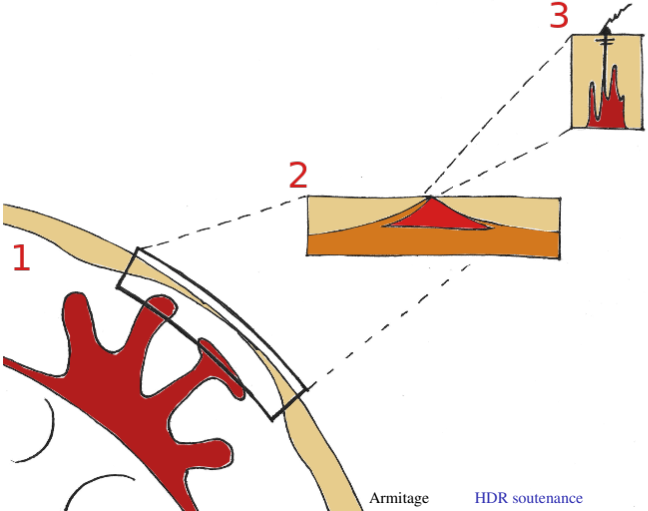

Thermal instabilities driven by hot base

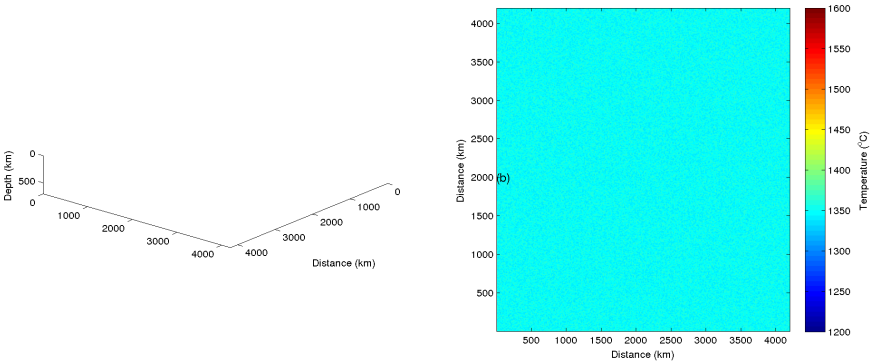

Figure: Thermal instabilities driven by a 100 °C hot base. Newtonian rheology, $T_P = 1350\,°\mathrm{C}$; $Ra = 6 \times 10^6$.

Thermal instabilities driven by hot base

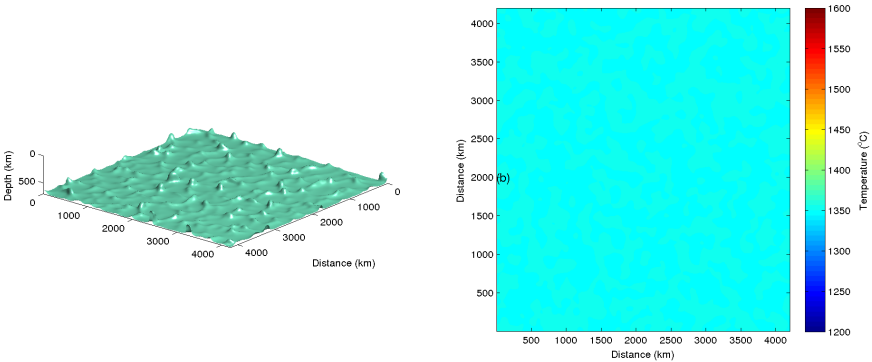

Figure: Thermal instabilities driven by a 100 °C hot base. Newtonian rheology, $T_P = 1350\,°\mathrm{C}$; $Ra = 6 \times 10^6$.

Thermal instabilities driven by hot base

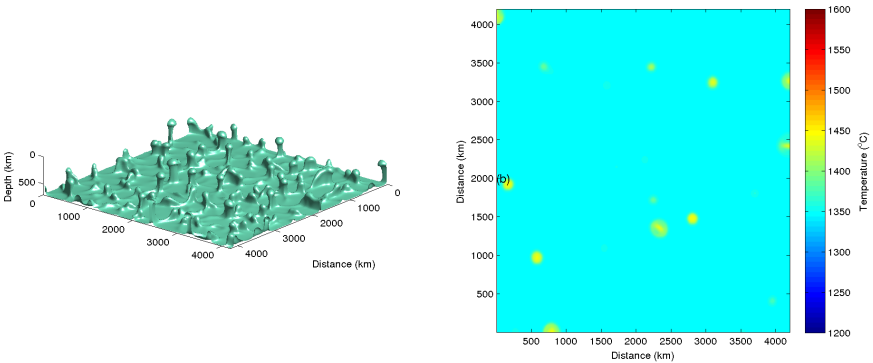

Figure: Thermal instabilities driven by a 100 °C hot base. Newtonian rheology, $T_P = 1350\,°\mathrm{C}$; $Ra = 6 \times 10^6$.

Thermal instabilities driven by hot base

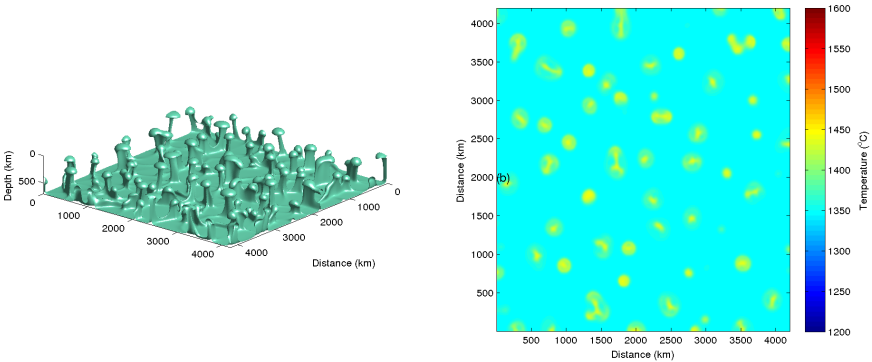

Figure: Thermal instabilities driven by a 100 °C hot base. Newtonian rheology, $T_P = 1350\,°\mathrm{C}$; $Ra = 6 \times 10^6$.

Thermal instabilities driven by hot base

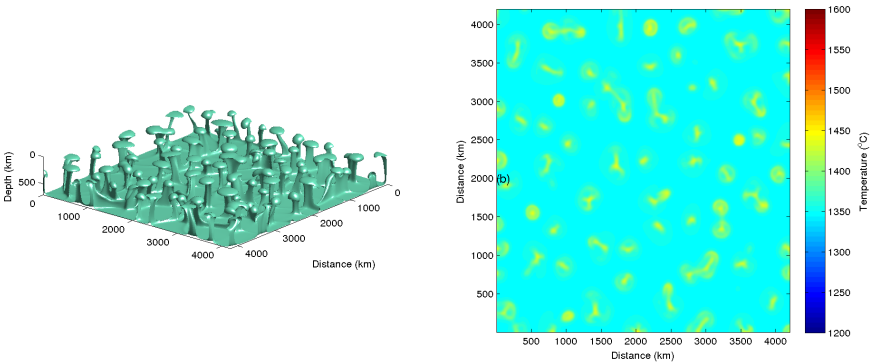

Figure: Thermal instabilities driven by a 100 °C hot base. Newtonian rheology, $T_P = 1350\,°\mathrm{C}$; $Ra = 6 \times 10^6$.

Thermal instabilities driven by hot base

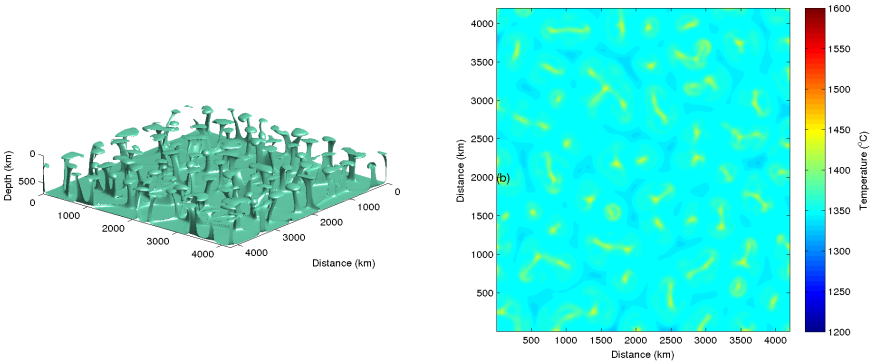

Figure: Thermal instabilities driven by a 100 °C hot base. Newtonian rheology, $T_P = 1350\,°\mathrm{C}$; $Ra = 6 \times 10^6$.

Thermal instabilities driven by hot base

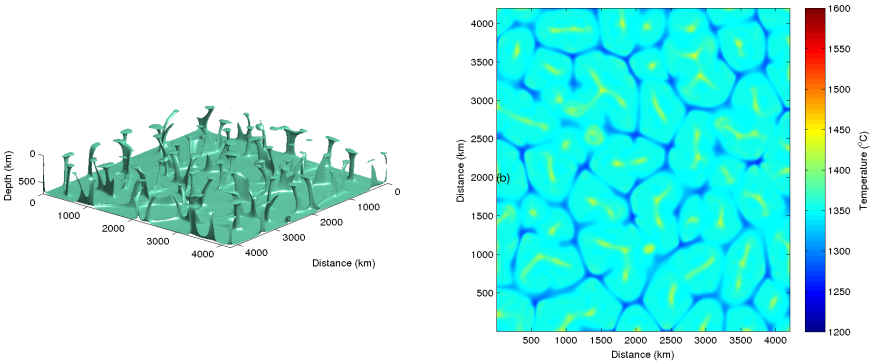

Figure: Thermal instabilities driven by a 100 °C hot base. Newtonian rheology, $T_P = 1350\,°\mathrm{C}$; $Ra = 6 \times 10^6$.

Thermal instabilities driven by hot base

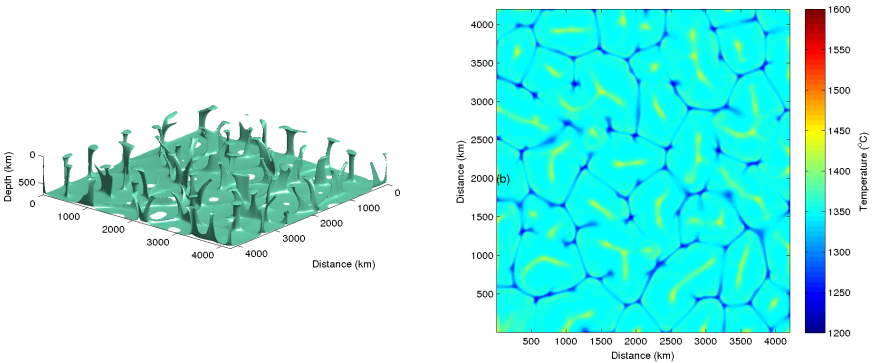

Figure: Thermal instabilities driven by a 100 °C hot base. Newtonian rheology, $T_P = 1350\,°\mathrm{C}$; $Ra = 6 \times 10^6$.

Relationship between Ra and λ

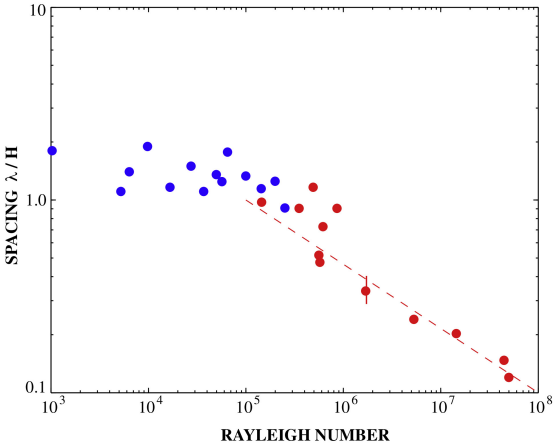

Figure: Laboratory experiments for temperature dependent viscosity suggests $\lambda \propto Ra^{-1/3}$ (Androvandi et al., 2011).

Relationship between Ra and λ

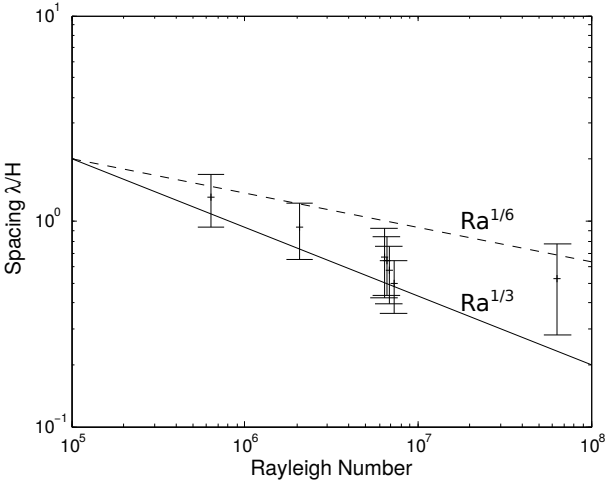

Figure: Numerical experiments for temperature dependent viscosity suggests $\lambda \propto Ra^{-1/3}$

Conversion of instabilities to V_S

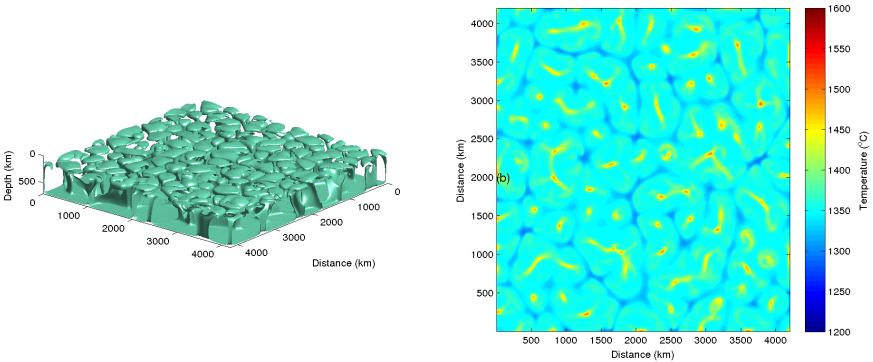

Figure: Thermal instabilities driven by a 200 °C hot base. Newtonian rheology, $T_P = 1350\,°\mathrm{C}$; $Ra = 6 \times 10^6$.

Conversion of melt and temperature to V_S

1. Anharmonic effects: Use composition to map out mineral phases and calculate velocity using PerPleX (Connolly, 2005).
2. Melt effect: Assume strongest effect: -7.9 % drop in velocity per percent porosity, ϕ, (Hammond and Humphreys, 2000).
3. Anelasticity: attenuation (Q) due to temperature (T) and dehydration C_{OH} due to melting,
   $Q = A_g \left(\frac{C_{OH}^{ref}}{C_{OH}} \right)^s \omega^\alpha exp \left(\frac{\alpha \gamma T_m}{T} \right)$.
4. This gives a seismic shear-wave velocity (V_S),
   $V_S = V_{\text{anh+melt}} \left(1 - \frac{Q^{-1}}{2tan(\pi\alpha/2)} \right)$.

Conversion of instabilities to V_S

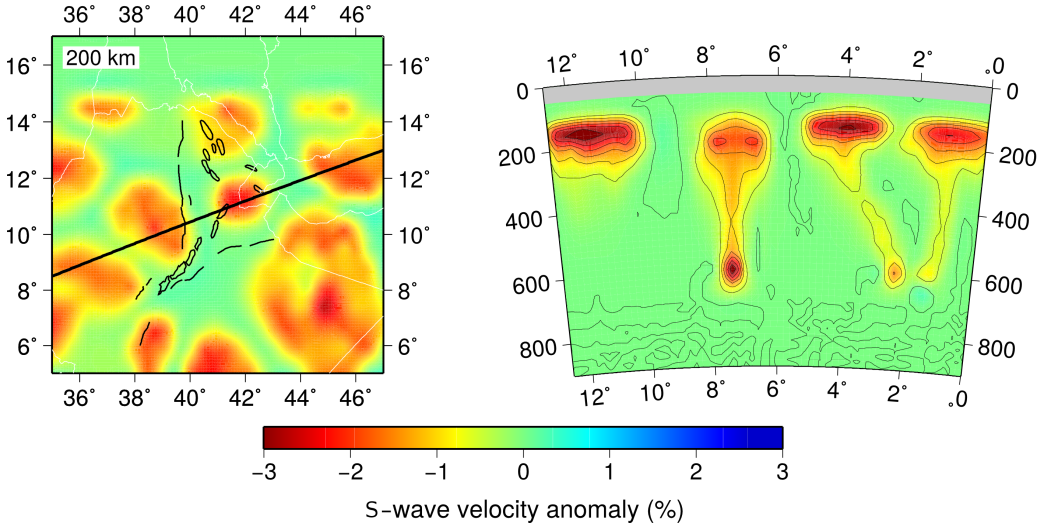

Figure: Model seismic structure of Rayleigh Bernard convection

Conversion of instabilities to synthetic tomography

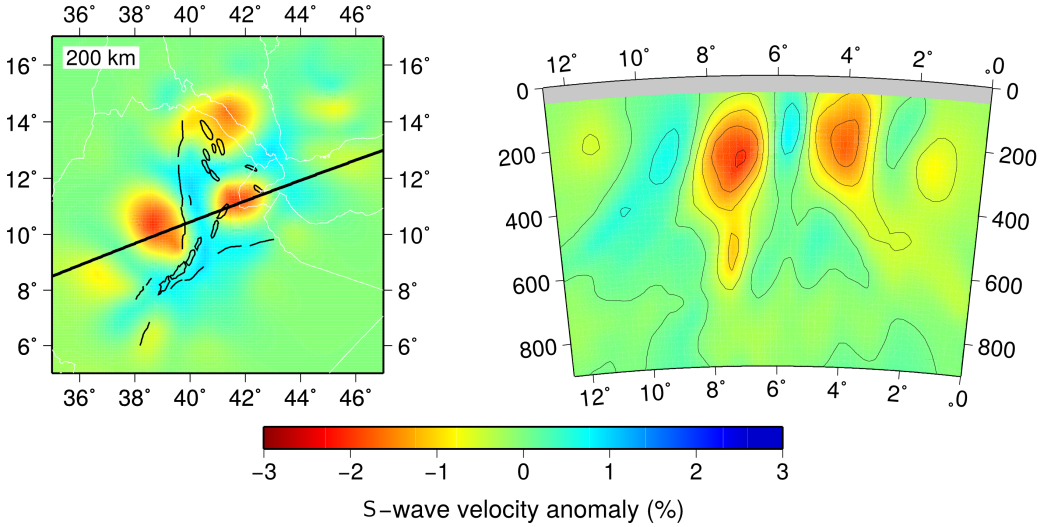

Figure: Rayleigh Bernard convection resolved by seismic array

Comparison of synthetic tomography

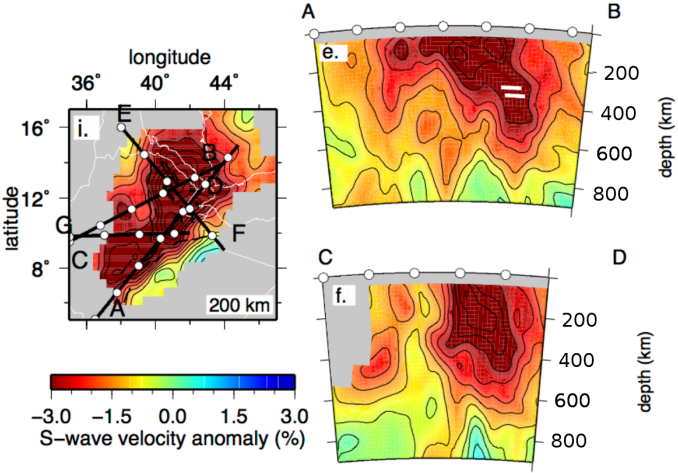

Figure: Rayleigh Bernard convection cannot create the gradient in velocity change that is seen in the inversion

Secondary plumes or destabilisation?

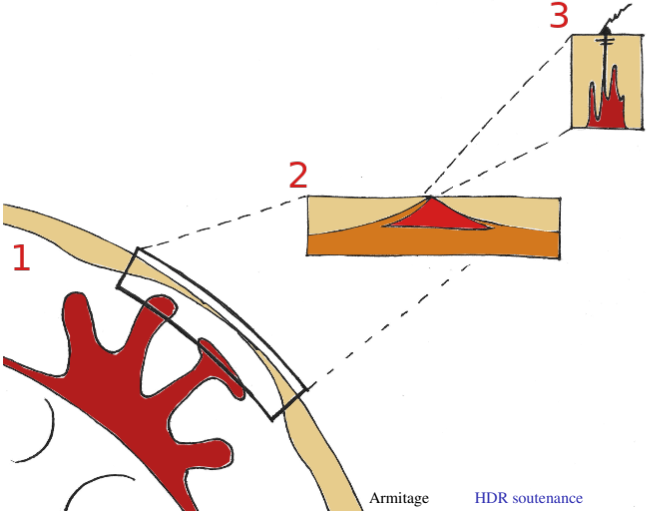

Destabilisation of a hot layer

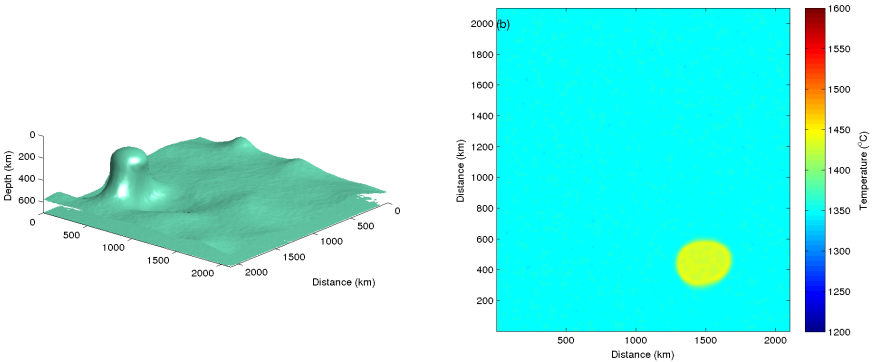

Figure: Destabilisation of a 100 °C hot layer, non-Newtonian rheology, $T_P = 1350\,°\mathrm{C}$; $Ra = 6 \times 10^6$.

Destabilisation of a hot layer

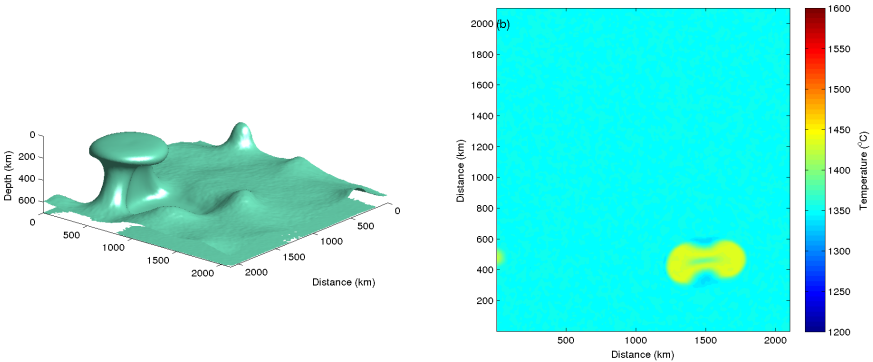

Figure: Destabilisation of a 100 °C hot layer, non-Newtonian rheology, $T_P = 1350\,°\mathrm{C}$; $Ra = 6 \times 10^6$.

Destabilisation of a hot layer

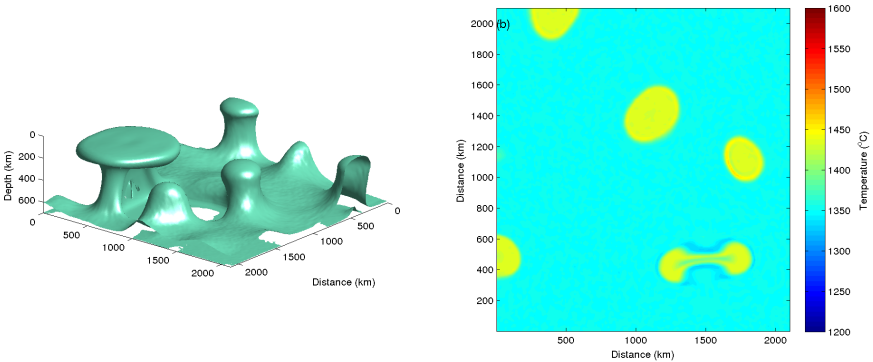

Figure: Destabilisation of a 100 °C hot layer, non-Newtonian rheology, $T_P = 1350\,°\mathrm{C}$; $Ra = 6 \times 10^6$.

Destabilisation of a hot layer

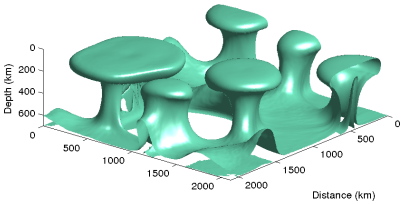

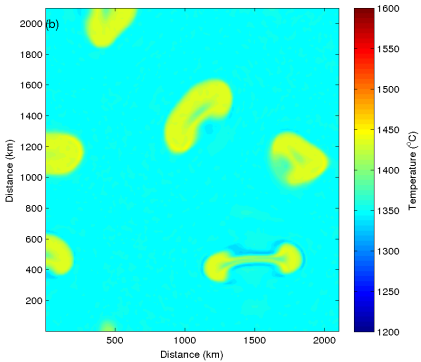

Figure: Destabilisation of a 100 °C hot layer, non-Newtonian rheology, $T_P = 1350\,°\mathrm{C}$; $Ra = 6 \times 10^6$.

Destabilisation of a hot layer

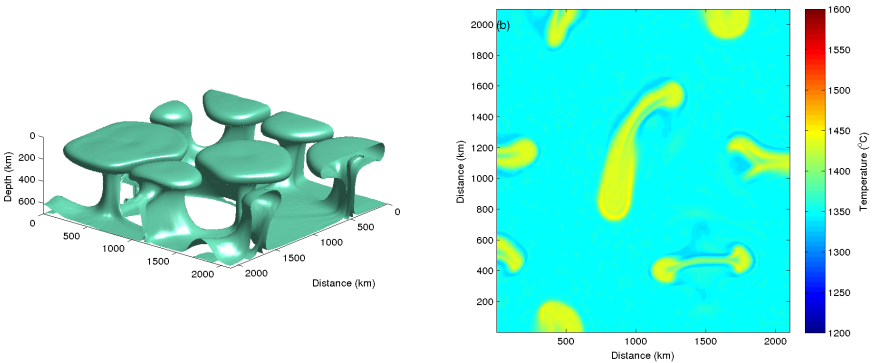

Figure: Destabilisation of a 100 °C hot layer, non-Newtonian rheology, $T_P = 1350\,°\mathrm{C}$; $Ra = 6 \times 10^6$.

Destabilisation of a hot layer

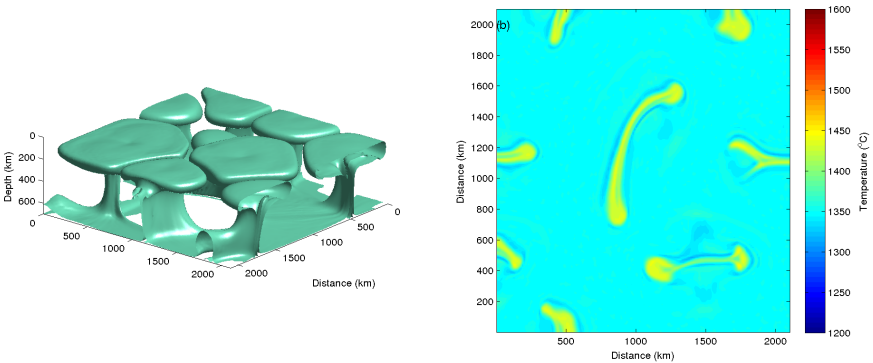

Figure: Destabilisation of a 100 °C hot layer, non-Newtonian rheology, $T_P = 1350\,°\mathrm{C}$; $Ra = 6 \times 10^6$.

Destabilisation of a hot layer

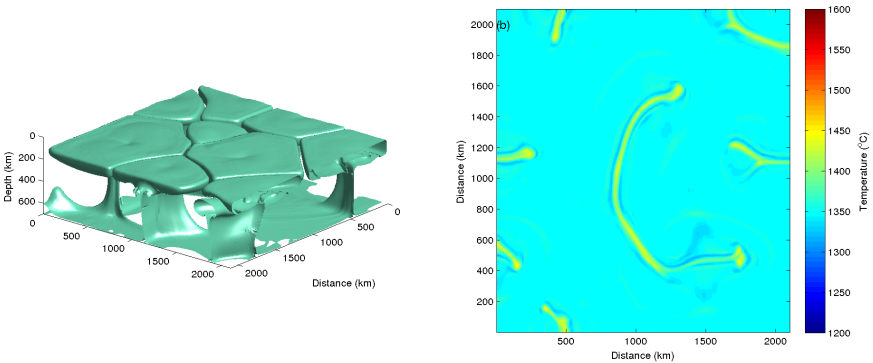

Figure: Destabilisation of a 100 °C hot layer, non-Newtonian rheology, $T_P = 1350\,°\mathrm{C}$; $Ra = 6 \times 10^6$.

Destabilisation of a hot layer: different stages of plume evolution

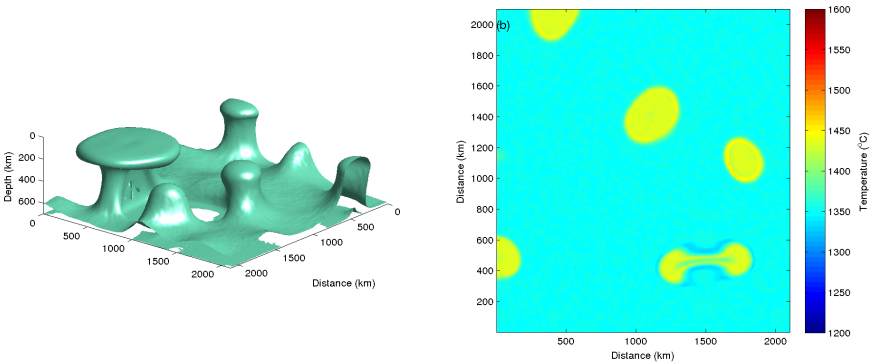

Figure: Destabilisation of a 100 °C hot layer, non-Newtonian rheology, $T_P = 1350\,°\mathrm{C}$; $Ra = 6 \times 10^6$.

Model - Tomography Comparison

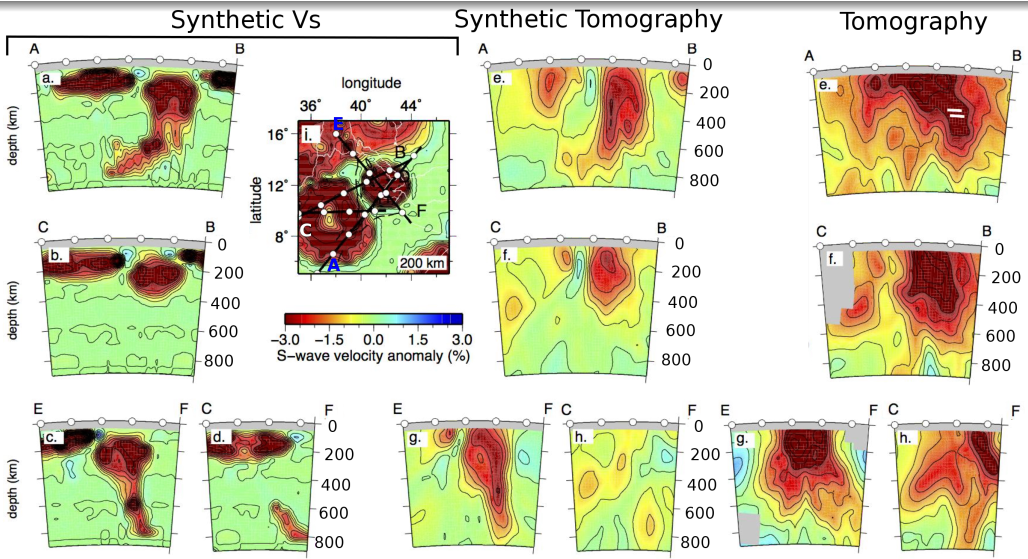

‘Plumelets’ below the Northern East African Rift

- Despite trying everything the seismic inversion cannot be recreated by Rayleigh Bernard convection.
  - *Plumelets have a temperature contrast that is too diffuse when resolved at the resolution of the seismic experiment.*
  - *Plumelets with a non-Newtonian rheology have very thin tails that are invisible at the resolution of the seismic experiment.*
- The destabilisation of a hot layer of mantle material best describes the tomographic model.
  - *This however requires material to pond below the 660 discontinuity and then destabilise.*
  - *Therefore the plumelets must be distinct from the background upper mantle.*
- For more see Civiero et al. (2020). Work in collaboration with Chiara Civiero, Saskia Goes and James Hammond.

Part 1.2: Melt generation at zones of extension

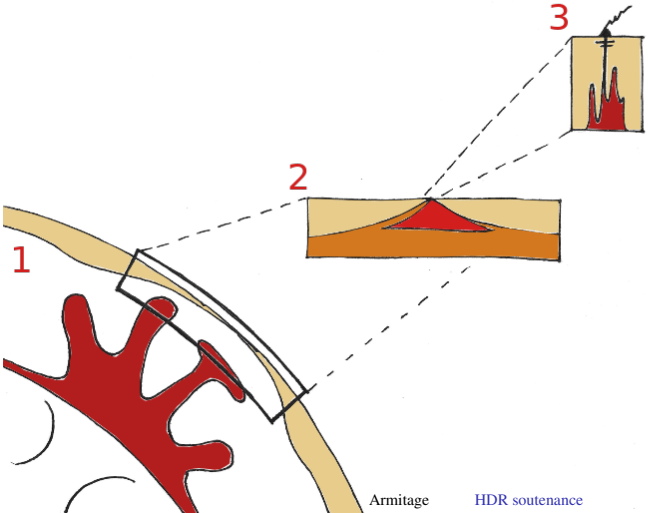

Northern East African Rift

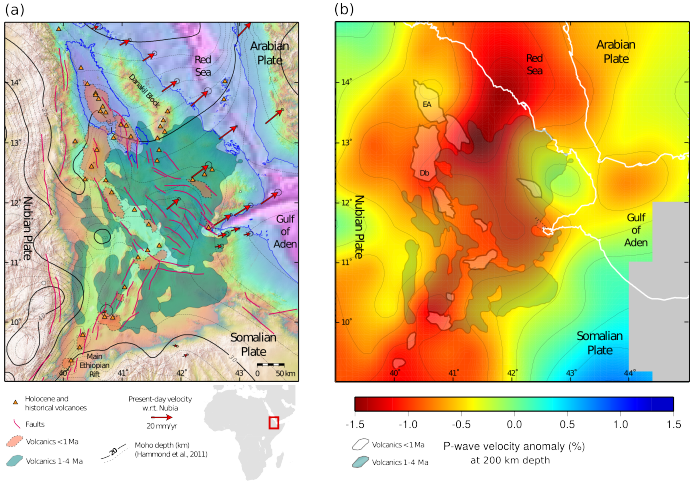

Figure: Narrow topographic expression of rifting in the southwest. Explained by focused localisation of stress or pre-existing weakness?

Armitage HDR soutenance

Modelling decompression melting

1. Stokes flow and Boussinesq approximation
2. Decompression melt production ($\dot{m}$) and tracing of mantle composition (C_S), $\dot{C}_S + \mathbf{V}_S.\nabla C_S = \left(1 - \frac{1}{D}\right) \frac{C_S}{\rho(1-\phi)} \dot{m}$.
3. Solve in a 2D domain with extension applied as a kinematic boundary condition that deforms the domain.
4. Model developed with Kenni Petersen

Visoc-elasto-plastic model with melting

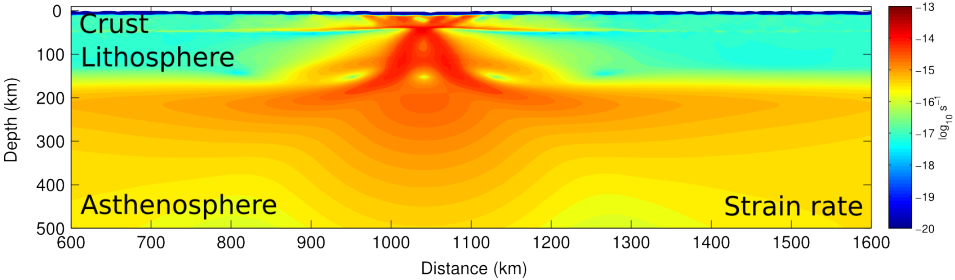

Figure: Example of stress field during extension which can be driven by force or velocity boundary conditions

Visoc-elasto-plastic model with melting

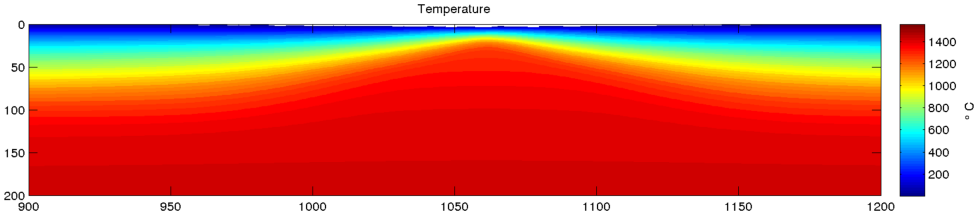

Figure: Extension at 5 mm yr^{-1} for 25 Myr with a mantle potential temperature of 1350 °C

Visoc-elasto-plastic model with melting

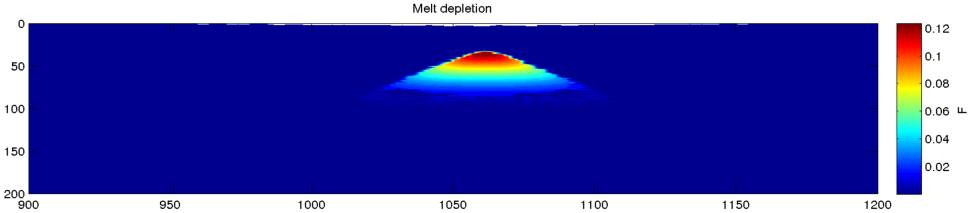

Figure: Melt depletion at 5 mm yr^{-1} for 25 Myr with a mantle potential temperature of 1350 °C

Visoc-elasto-plastic model to seismic structure

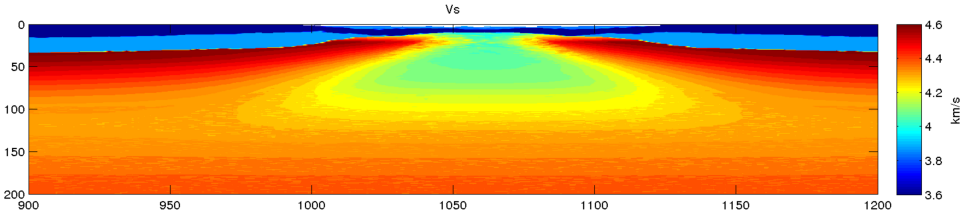

Figure: Seismic velocity at 5 mm yr^{-1} for 25 Myr with a mantle potential temperature of 1350 °C

Visoc-elasto-plastic model to seismic structure

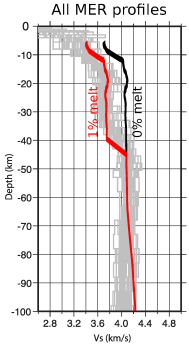

Figure: Comparison of the predicted S-wave seismic velocity from the forward model and the ensemble vertical profiles from the joint inversion of Rayleigh waves and receiver functions below the Main Ethiopian Rift (Keranen et al., 2009). The black line is the model V_S assuming no melt storage, the red line assumes that 1 % melt is stored above 40 km depth.

Part 1.3: Melt transport and deglaciation

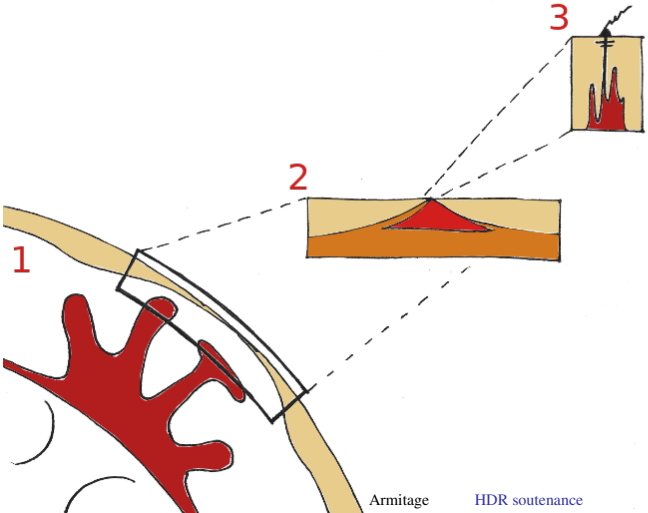

Melt retention and melt velocity: a trade off

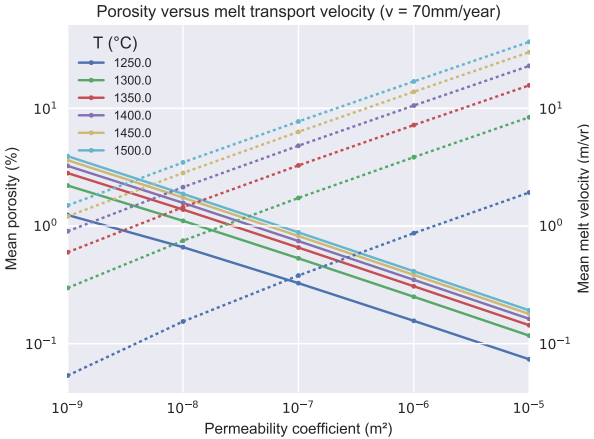

Figure: To have high melt retention requires slow melt transport (Franken et al., 2020). However, it is often reported that melt generation responds to climatic forcing.

Iceland: Melt generation since last glacial maximum (LGM)

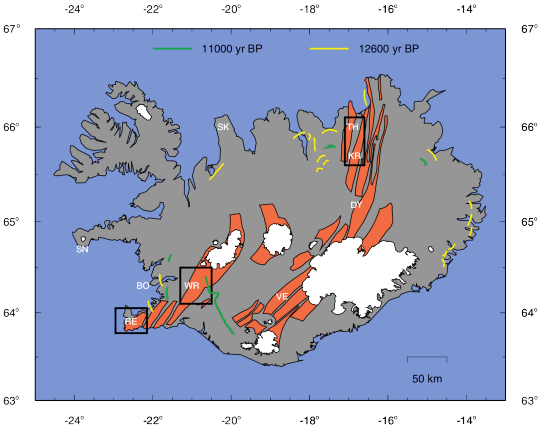

Figure: Distribution of basalt flows and limits of ice-sheet (Maclennan et al., 2002)

Iceland: Melt generation since last glacial maximum (LGM)

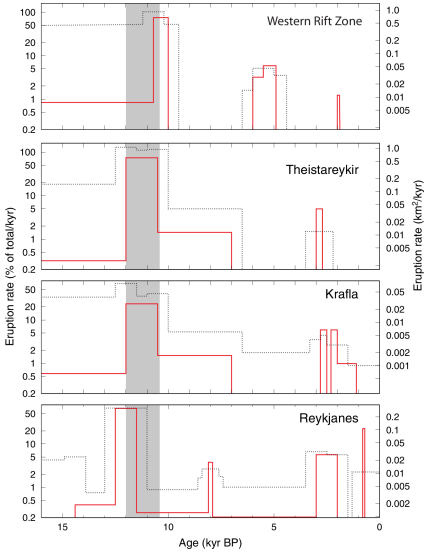

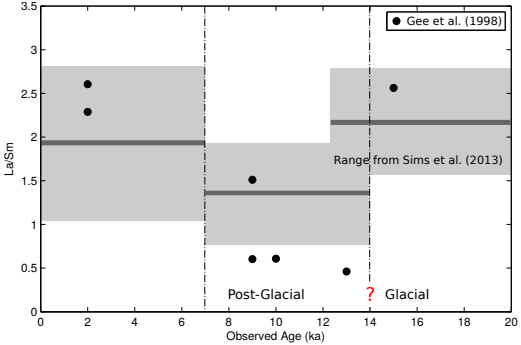

Change in La and Sm concentrations since LGM. Low La/Sm due to increased shallow melt production?

Solve for vertical flow of melt

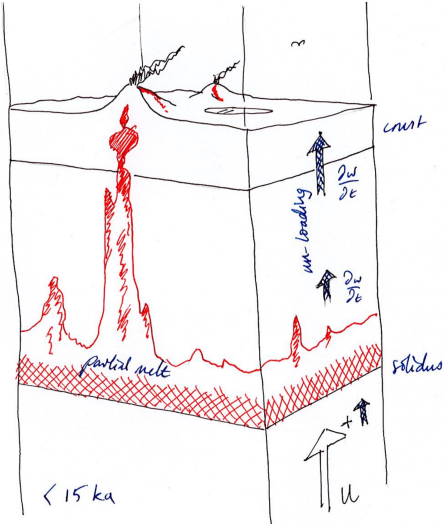

Define an average velocity,

$$\bar{v} = (1-\phi)v_s + \phi v_l,$$

and this velocity is given by the rate of up-welling plus the rate of change of displacement due to loading (unloading),

$$\bar{v} = u + \frac{\partial w}{\partial t},$$

where u is the rate of up-welling.

Solve for vertical flow of melt

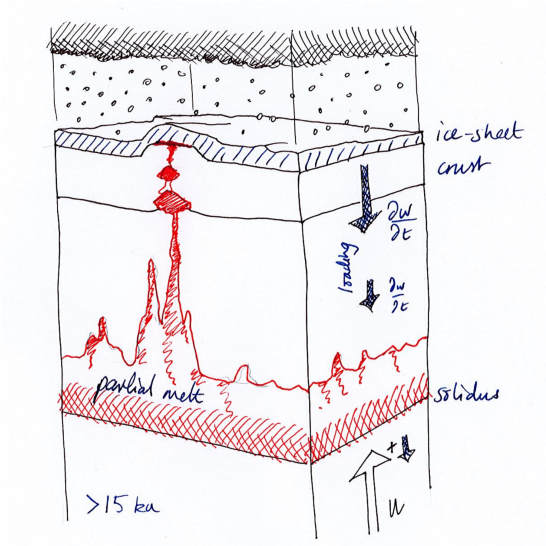

$$\bar{v} = u + \frac{\partial w}{\partial t},$$

where $\partial w/\partial t$ is the rate of change in vertical displacement. This is calculated from the change in surface displacement, w_0,

$$\frac{ET_e}{12\left(1-\mu^2\right)}\frac{\partial^4}{\partial x^4}\left(\frac{\partial w_0}{\partial t}\right) = \frac{P_{ice}}{\tau_e},$$

P_{ice} is the load due to an ice-sheet, and $\tau_e = 3\eta_s/E$ is the viscous response time. This displacement decays with depth as,

$$\frac{\partial w}{\partial t} = \frac{\partial w_0}{\partial t} exp\left(-\sqrt{3}\pi\frac{z}{\lambda}\right),$$

where λ is the width of the ice-sheet.

Solve for vertical flow of melt

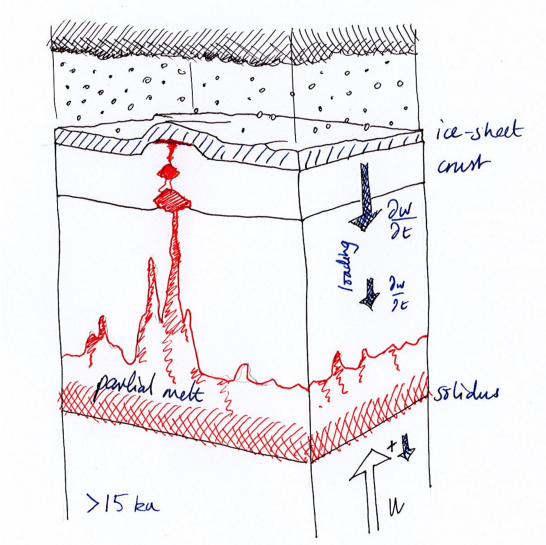

Conservation of energy,

$$mL + \frac{\partial T}{\partial t} + \bar{v}\frac{\partial T}{\partial z} - \kappa\frac{\partial^2 T}{\partial z^2} = 0.$$

Conservation of mass for the melt,

$$\frac{\partial \phi}{\partial t} + \frac{\partial}{\partial z}\left(\phi v_l\right) = m.$$

Darcy's law (assuming zero-compaction length),

$$\phi\left(v_l - v_s\right) = \frac{k_0 \phi^n}{\eta_l}\Delta\rho g.$$

Solve for vertical flow of melt

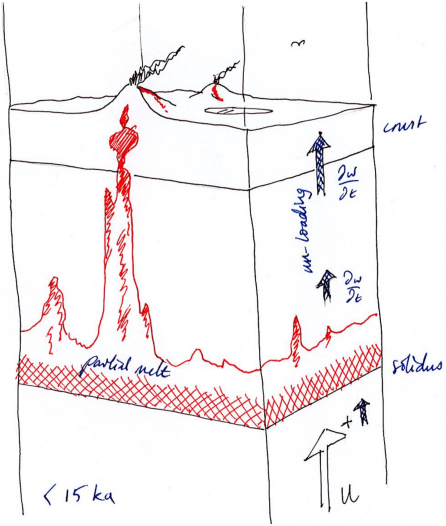

Use the definition of average velocity, Darcy's law,

$$\phi\left(v_l - v_s\right) = \frac{k_0 \phi^n}{\eta_l} \Delta\rho g,$$

assuming $n = 3$, and conservation of mass to get,

$$\frac{\partial \phi}{\partial t} + \bar{v}\frac{\partial \phi}{\partial z} + \frac{3k_0 \Delta\rho g}{\eta_l}\phi^2\left(1 - \frac{4}{3}\phi\right)\frac{\partial \phi}{\partial z} = m.$$

We have one unknown, ϕ, where melt production rate m is calculated from the temperature difference to the solidus.

Impact of permeability on melt storage and simulated seismic velocity

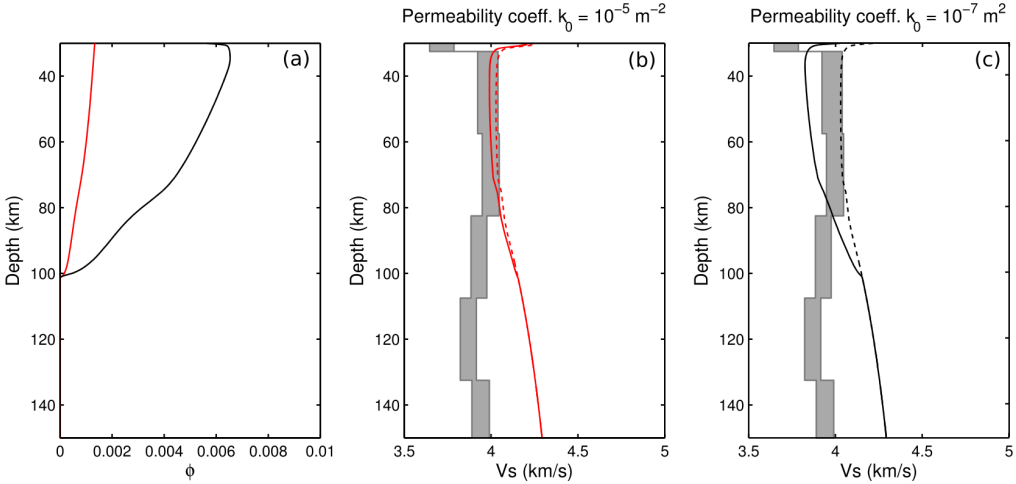

Figure: Profiles of porosity and seismic velocity for the 1D model.

Simulated melt eruption rates for the Holocene

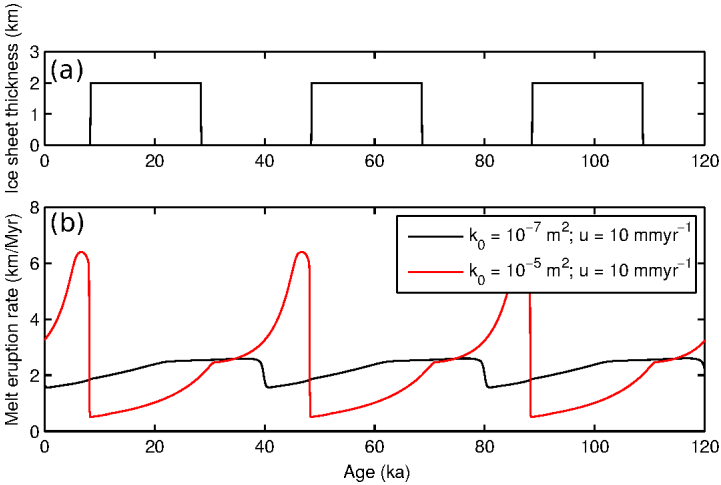

Figure: For the model to respond rapidly to deglaciation the permeability coefficient needs to be high, $k_0 = 10^{-5}$

Simulated melt eruption rates for the Holocene

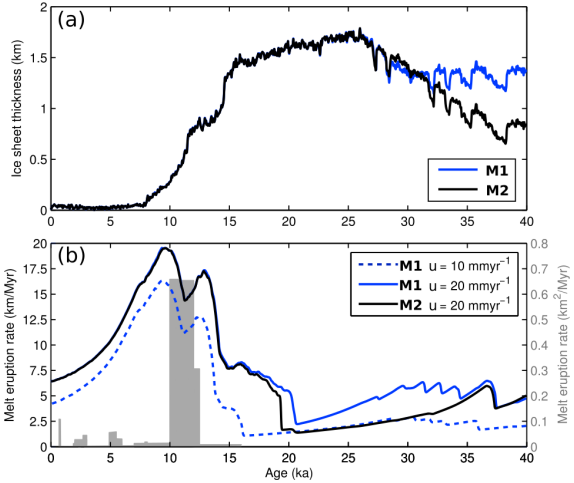

Figure: For the model to respond rapidly to deglaciation the permeability coefficient needs to be high, $k_0 = 10^{-5}$

Melt retention and melt velocity: a trade off

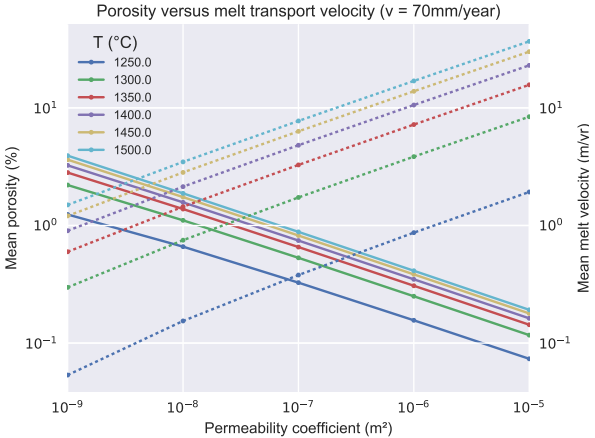

Visoc-elasto-plastic model to seismic structure

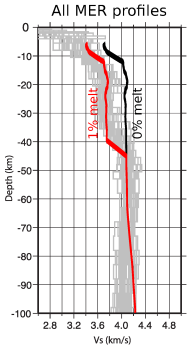

Figure: The black line is the model V_S assuming no melt storage, the red line assumes that 1 % melt is stored above 40 km depth, **but how can we both have high storage and fast transport?**

Questions not conclusions

- We cannot have both a system that responds to climate change and stores melt.
- What if the model of McKenzie for the compaction and transport of melt is not appropriate?
- Does melt flow localise into channels, flow like rivers through the matrix?

Part 2: Rivers

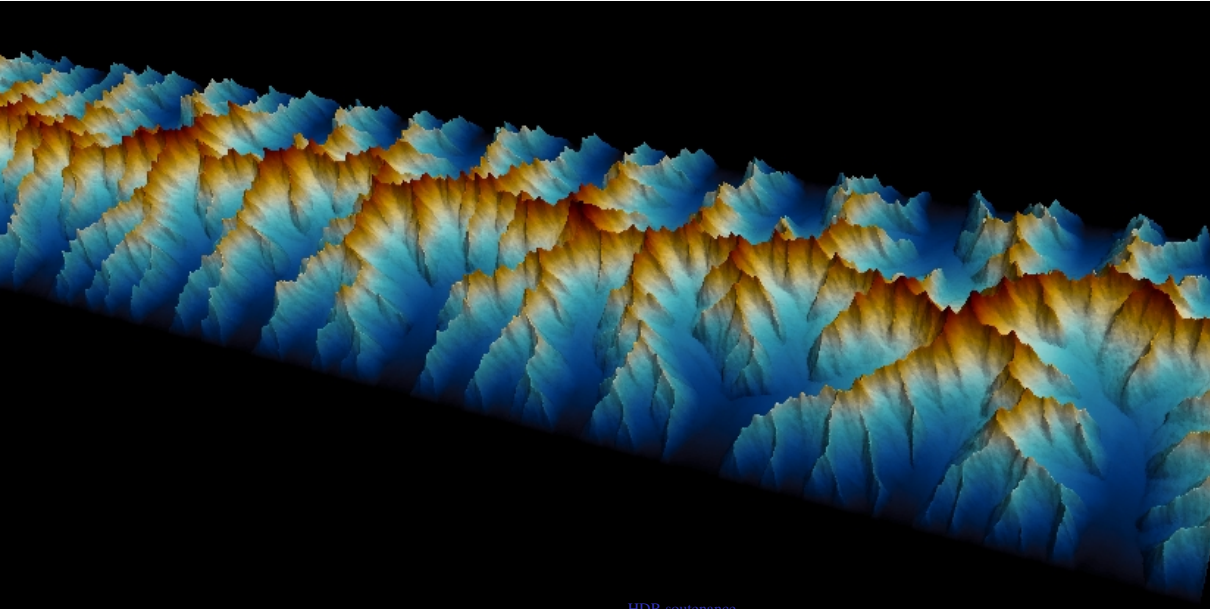

Width of a river relative to the width of a cell

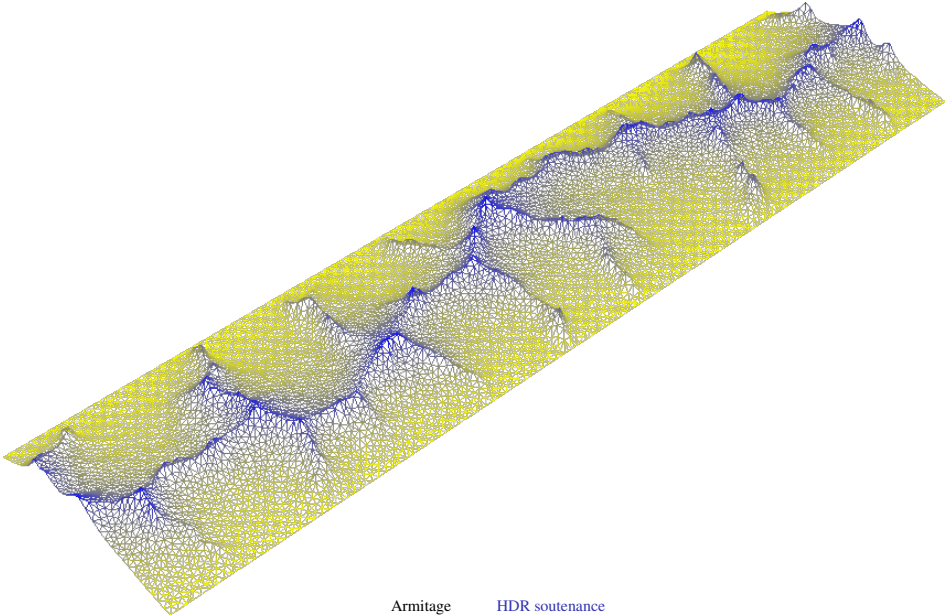

Width of a river relative to the width of a cell

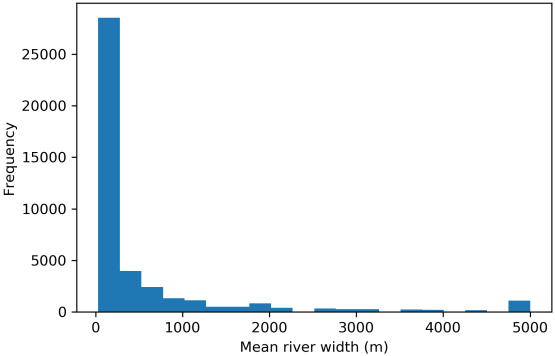

- Distribution of mean river width taken from the Global River Widths from Landsat (GRWL) Database (Allen and Pavelsky, 2018)
- How do we model the transport of sediment by flowing water? At a scale smaller or larger than a river?

A landscape evolution model

One of the simplest landscape evolution models can be derived if we assume erosion and deposition occur due to the transport of sediment across the surface of the Earth.

$$\frac{\partial z}{\partial t} = \nabla \mathbf{q_s} + U$$

and that sediment flux is a function of the water flux,

$$\mathbf{q_s} = -\left[\kappa \nabla z + c\mathbf{q_w} \cdot \nabla z\right]$$

but how to route water?

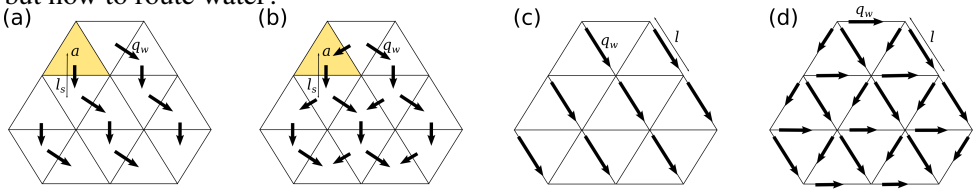

cell-to-cell steepest descent | cell-to-cell distributed | node-to-node steepest descent | node-to-node distributed

Single Flow Direction (SFD; steepest descent) cell to cell

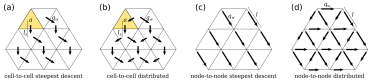

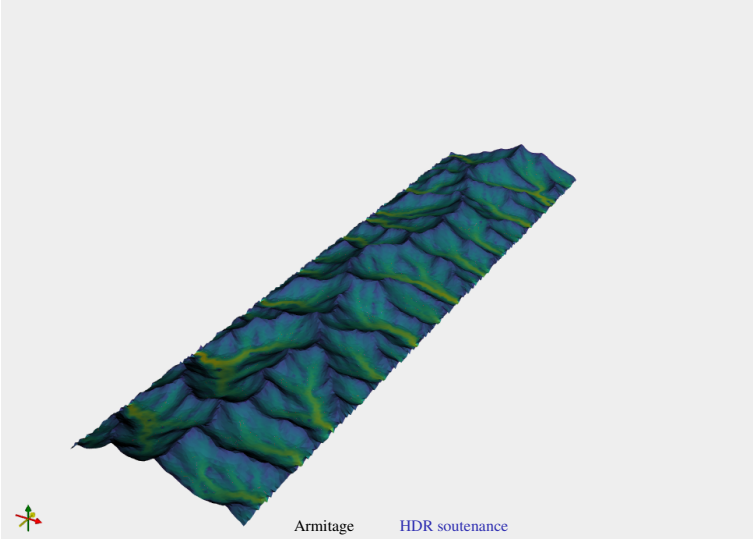

Single Flow Direction (SFD; steepest descent) node to node

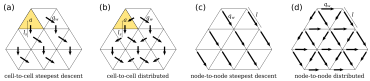

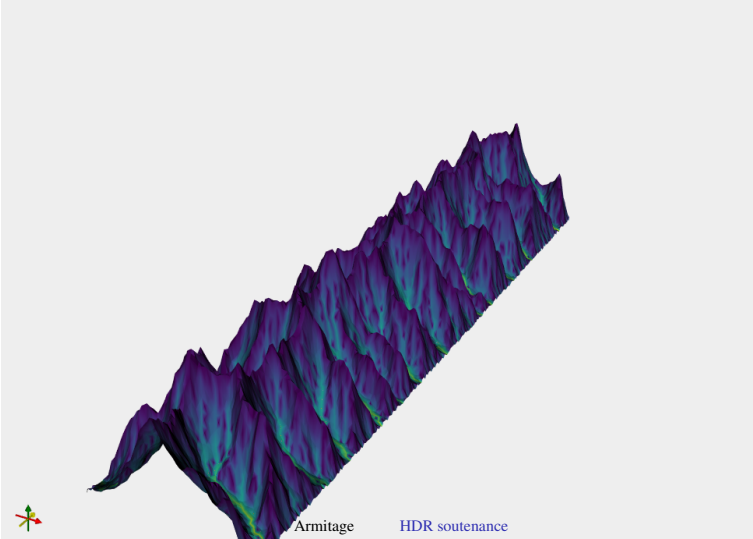

Multiple Flow Direction (MFD; distributed) cell to cell

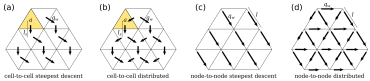

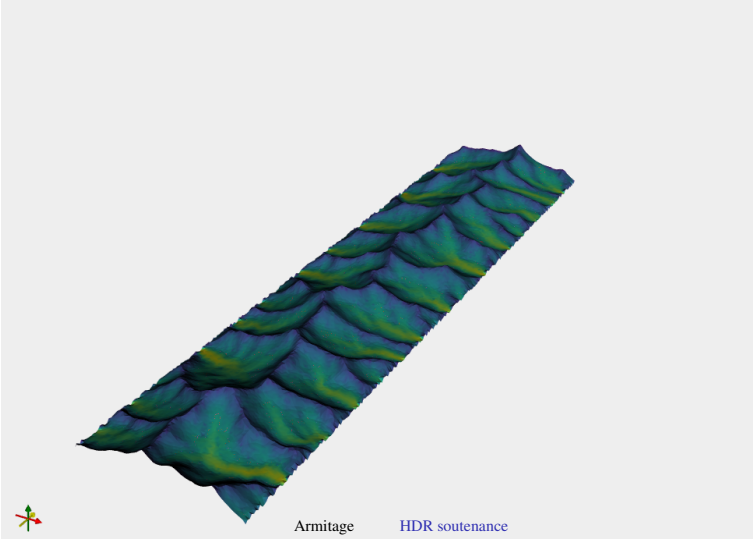

Multiple Flow Direction (MFD; distributed) node to node

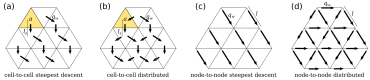

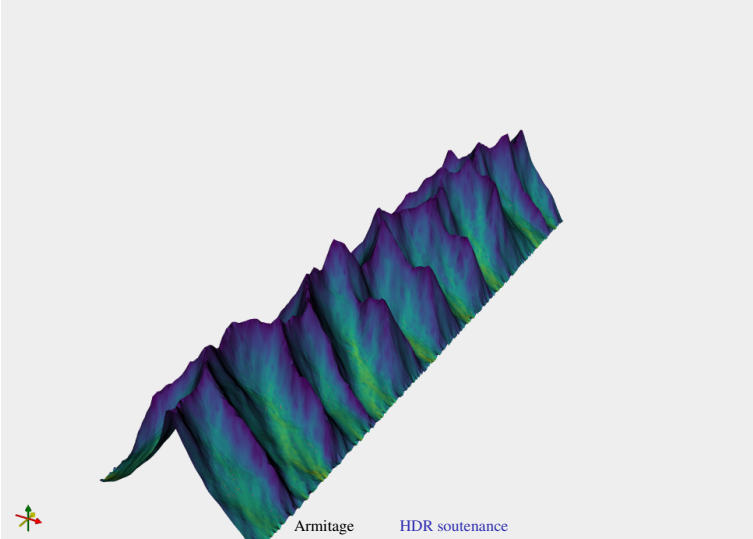

Valley to valley wavelength

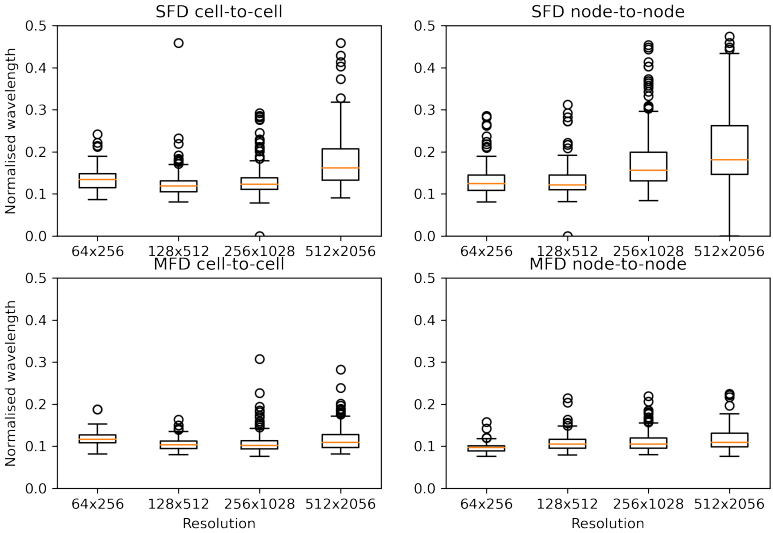

Sediment flux through time

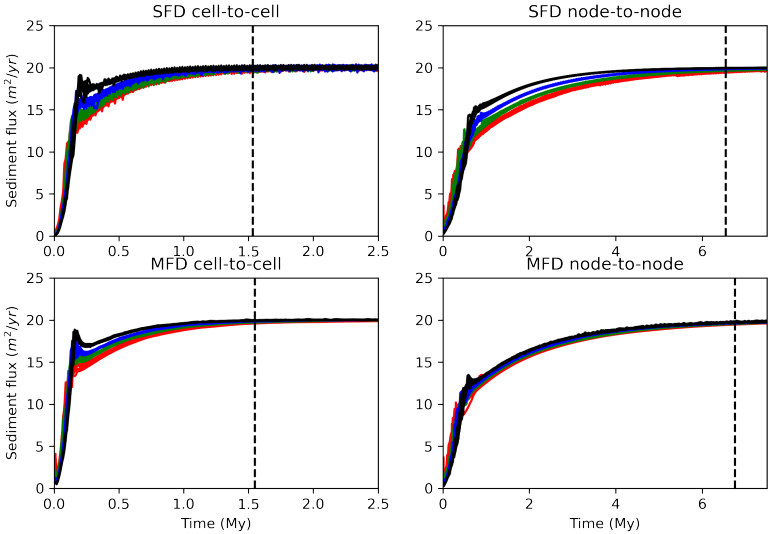

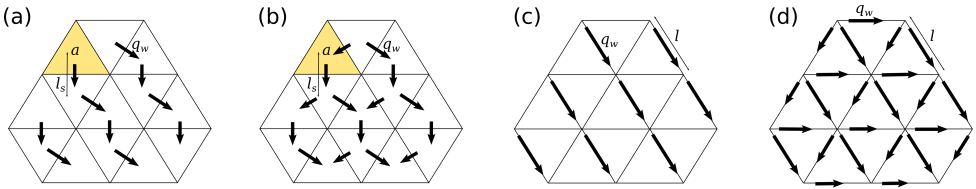

cell-to-cell steepest descent | cell-to-cell distributed | node-to-node steepest descent | node-to-node distributed

- MFD node-to-node resolves the resolution dependence
- The flow of water is therefore being treated as going down 1D lines distributed over multiple (<6) directions
- Most LEMs assume a single flow direction as it is expedient, but water does not flow down slope in such a simple manner.
- Should LEMs start to consider how water really flows through the landscape?

Rivers and Melt

- In both parts, melt transport and landscape evolution, the models are on a scale far greater than the processes. Simplifying assumptions must be made. Yet in both cases the physics of the processes at a scale below the model grid cannot be ignored.
- Classic Darcy flow through a permeable matrix cannot explain the ensemble of observations:
  the seismic observations tend to require a longer travel time delay that can be explained by melt retention alone
- Landscape evolution models cannot overlook processes at the scale of a river:
  we need to numerically distribute the water to all down slope cells, but in nature water flows through the landscape not on top of it.
- It is only by comparing the models with observations that the importance of these processes becomes clear.

What next: Groundwater

Physical model → Seismic velocity → Seismic observation

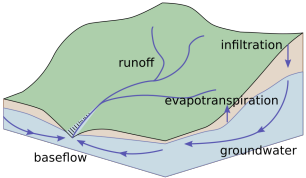

Explore change in velocity due to groundwater

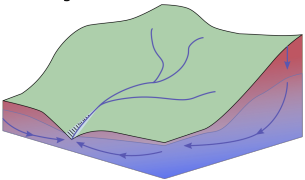

Example inversion of change in seimsic velocity from 17 years of ambient seismic noise in the in San Gabriel Valley (Clements & Denolle, 2018)

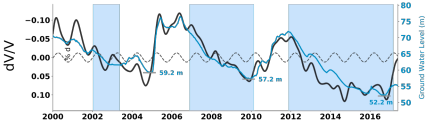

Surface and groundwater

- Roughly 40 % of water is transported in the subsurface. This transport is not captured by landscape evolution models.
- In steep and high mountain catchments this store of water is of vital importance

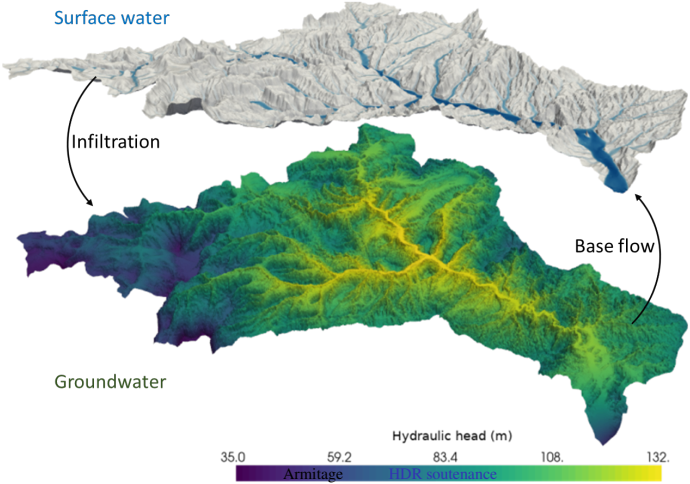

Passive seismic monitoring of groundwater

- Focus on the Bhote Koshi catchment in Nepal

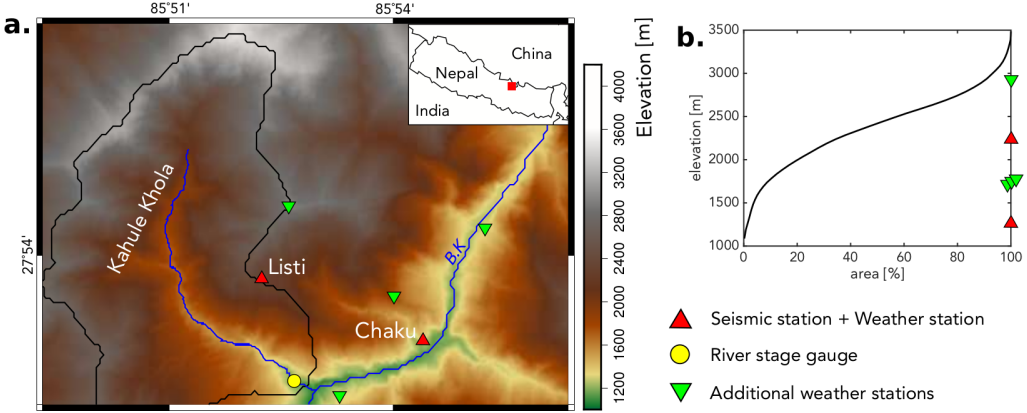

Passive seismic monitoring of groundwater

- Change in the groundwater levels is reflected in the cross-correlation of ambient seismic noise (Illien et al., 2021)

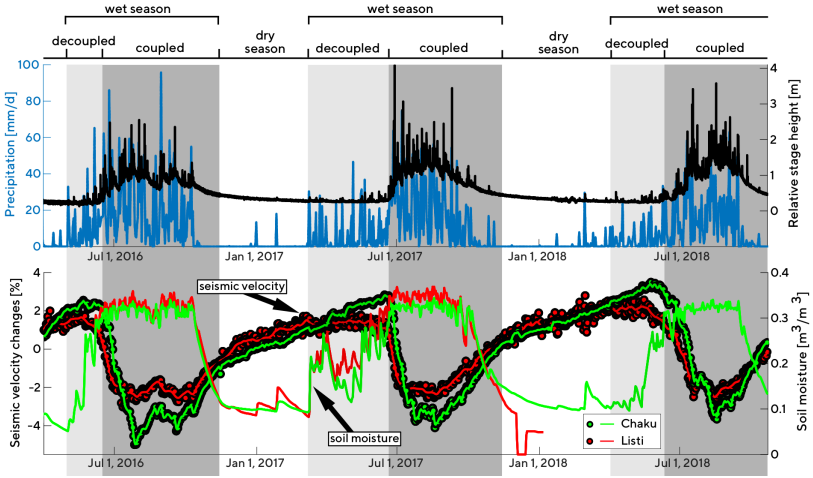

Armitage HDR soutenance

PhD project starting in December

- Develop methods to couple surface and groundwater flow
- Use existing observations from Nepal to explore model assumptions and hypothesis
- Collaboration with Niels Hovius, Christoff Andermann, and Nobu Fuji

Physical model → Seismic velocity → Seismic observation

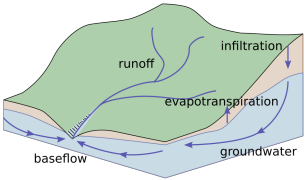

Explore change in velocity due to groundwater

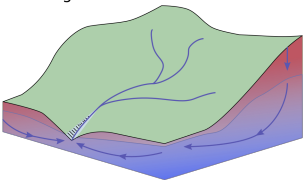

Example inversion of change in seimsic velocity from 17 years of ambient seismic noise in the in San Gabriel Valley (Clements & Denolle, 2018)

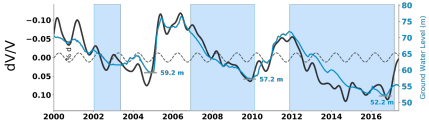

References

Allen, G. H., Pavelsky, T. M., 2018. Global extent of rivers and streams. Science 361, 585–588, doi: 10.1126/science.aat0636.

Androvandi, S., Davaille, A., Limare, A., Foucquier, A., Marais, C., 2011. At east three scales of convection in a mantle with strongly temperature dependent viscosity. Physics of the Eath and Planetary Interiors 188, 132–141, doi: 10.1016/j.pepi.2011.07.004.

Civiero, C., Armitage, J. J., Goes, S., Hammmond, J. O. S., 2020. The seismic signature of upper-mantle plumes: application to the northern east african rift. Geochemistry Geophysics Geosystems 20, 6106–6122, doi: 10.1029/2019GC008636.

Civiero, C., Goes, S., Hammond, J. O. S., Fishwick, S., Ahmed, A., Ayele, A., Doubre, C., Goitom, B., Keir, D., Kendall, J. M., Leroy, S., Ogubazghi, G., Rümpker, G., Stuart, G. W., 2016. Small-scale thermal upwellings under the northern East African Rift from S travel time tomography. Journal of Geophysical Research 121, 7395–7408, doi: 10.1002/2016JB013070.

Connolly, J. A. D., 2005. Computation of phase equilibria by linear programming: A tool for geodynamic modelling and its application to subduction zone decarbonation. Earth and Planetary Science Letters 236, 524–541, doi:10.1016/j.epsl.2005.04.033.

Franken, T., Armitage, J. J., Fuji, N., Fournier, A., 2020. Seismic wave-based constraints on geodynamical processes: an application to partial melting beneath the Réunion island. Geochemistry, Geophysics, GeosystemsDoi: TBA.

Hammond, W. C., Humphreys, E. D., 2000. Upper mantle seismic wave velocity: Effects of realistic partial melt geometries. Journal of Geophysical Research 105, 10975–10986.

Illien, L., Anderman, C., Sens-Schönfelder, C., Cook, K. L., Baidya, K. P., Adhikari, L. B., Hovius, N., 2021. Subsurface moisture regulates Himalayan groundwater storage and discharge. AGU Advances 2, doi: 10.1029/2021AV000398.

Keranen, K. M., Klemperer, S. L., Julia, J., Lawrence, J. F., Nyblade, A. A., 2009. Low lower crustal velocity across Ethiopia: Is the Main Ethiopian Rift a narrow rift in a hot craton? Geochemistry Geophysics Geosystems 10 (5), doi: 10.1029/2008GC002293.

Maclennan, J., Jull, M., McKenzie, D., Slater, L., Grönvold, K., 2002. The link between volcanism and deglaciation in Iceland. Geochemistry Geophysics Geosystems 3 (11, 1062), doi: 10.1029/2001GC000282.

White, R. S., McKenzie, D., 1995. Mantle plumes and flood basalts. Journal of Geophysical Research 100, 17543–17585.